2021

Measurement of Condensation Heat Transfer and Pressure Drop for Zeotropic Mixture R-454C and its Components R-32 and R-1234yf in a Horizontal Microfin Tubes

Ethan P. Matty
Oregon State University, United States of America

Brian M. Fronk
Oregon State University, United States of America, brian.fronk@oregonstate.edu

A Comparison of Condensation Heat Transfer and Pressure Drop for Zeotropic Mixture R-454C and its Components, R-32 and R-1234yf, in a Horizontal Microfin Tube

Ethan P. MATTY[1], Brian M. FRONK[2*]

[1] School of Mechanical, Industrial and Manufacturing Engineering
Oregon State University
Corvallis, OR, United States
mattye@oregonstate.edu

[2] School of Mechanical, Industrial and Manufacturing Engineering
Oregon State University
Corvallis, OR, United States
Brian.Fronk@oregonstate.edu

* Corresponding Author

ABSTRACT

This paper compares the condensation heat transfer and pressure drop for zeotropic refrigerant R-454C and its individual components, R-32 and R-1234yf, in a horizontal microfin tube. The microfin tube has a 4 mm outer diameter, 0.18 mm wall thickness, and a surface area ratio of 1.56. HFOs and HFC/HFO blends like R-454C have low global warming potential and can be alternatives to HFC refrigerants when retrofitting a system or producing new equipment. However, there is an additional mass transfer resistance present during phase change for a zeotropic mixture, which results in reduced heat transfer performance. Microfin tubes enhance heat transfer through multiple mechanisms: they increase the internal surface area of the tube, the fins drain condensate from the fin tip to the trough region, and they produce secondary flow structures.

Presently, there is limited data of HFO/HFC mixtures in microfin tubes. Thus, experiments are conducted for complete condensation of R-454C, R-1234yf and R-32 for saturation temperatures of 40, 50 and 60 °C and mass fluxes from 100 to 600 $\mathrm{kg\,m^{-2}\,s^{-1}}$. Experimental heat transfer and pressure drop measurements are compared to well-established correlations from the literature. Heat transfer enhancement factors and pressure drop penalty factors are calculated for each refrigerant.

1. INTRODUCTION

Internal microfin tubes are widely used in the HVAC industry to provide condensation and evaporation heat transfer enhancement with minimal increase in pressure drop. Microfin tubes have internal fins that are typically less than a millimeter tall, helix angles from 15 – 40°, and 36-82 fins depending on the tube diameter. The fins enhance condensation heat transfer by increasing the internal surface area of the tube, producing secondary flow patterns, and draining condensate from the tip of the fin to the trough region.

Refrigerant regulations, such as the Kigali amendment to the Montreal Protocol and the EU F-gas regulations have driven the adoption of environmentally friendly refrigerant mixtures designed to replace refrigerants with high global warming potential (GWP). HFO-HFC zeotropic mixtures are attractive replacements because the mixture composition can be adjusted to meet environmental regulations while maintaining desirable thermophysical properties. However, there is a degradation in heat transfer performance of a mixture due to the additional mass transfer and sensible resistances that are present during zeotropic mixture condensation. Microfin tubes can potentially counteract the degradation in condensation heat transfer performance associated with a zeotropic mixture. Condensation and evaporation of pure fluids in microfin tubes has been widely investigated, but there are limited data for condensation of zeotropic mixtures in microfin tubes with diameters less than 8 mm.

Thus, in this study, we investigate the heat transfer and pressure drop characteristics of R-454C and its individual

Table 1: Experimental operating conditions for internal condensation in microfin tubes

Reference	Refrigerant	T_{sat} [°C]	G [kg m^{-2} s^{-1}]	D [mm]
Koyama et al. (1990)	22, 114, 22/114	36-54	130-360	8.32
Shizuya et al. (1995)	22/142b, 22/114, 22/123	47-77	188-738	7
Eckels and Tesene (1999a)	22, 134a, 410A, 407C	40, 50	125-600	7.94-15.88
Kedzierski and Goncalves (1999)	134a, 410A, 125, 32	22-51	85-500	9.5
Cavallini et al. (2002)	134a, 407C	40, 55	100-800	9.5
Han and Lee (2005)	134a, 22, 410A	18.5-33.8	91-1110	4-8.92
Kim and Shin (2005)	22, 410A	45	183-365	9.52
Cavallini et al. (2006)	410A	40	100-800	7.69
Wu et al. (2014)	410A	39-47	99-603	4.56-8.98
Diani et al. (2018)	1234yf, 1234ze(E)	30, 40	300-1000	3
Hirose et al. (2018)	32, 152a, 410A	35	100-400	4
Kondou (2019)	1123/32	40	200-400	6
Bashar et al. (2020)	1234yf	20, 30	50-200	2.5

components in a microfin tube over a range of operating conditions. Data are obtained for complete condensation of the mixture and its constituent components in a microfin tube with 4 mm outer diameter (OD), 0.18 mm wall thickness (s), with a surface area ratio of 1.56. We then evaluate the predictive capabilities of microfin condensation heat transfer and frictional pressure drop correlations from the literature.

2. PRIOR WORK

Several researchers have investigated the enhancement effects of microfin tubes for in-tube condensation. A summary of experimental operating conditions and microfin tube ODs from the literature are summarized in Table 1. It is evident that experimental data is sparse for next-generation zeotropic mixtures in small diameter tubes.

The heat transfer and pressure drop characteristics of microfin tubes are often compared to smooth tubes under the same operating conditions. The ratio of the heat transfer coefficient, α, in a microfin tube over a smooth tube is defined as the enhancement factor, shown in Equation 1. The penalty factor is defined analogously, but with frictional pressure drop, ΔP_{fr}, as shown in Equation 2.

$$EF = \frac{\alpha_{microfin}}{\alpha_{smooth}} \tag{1}$$

$$PF = \frac{\Delta P_{fr,microfin}}{\Delta P_{fr,smooth}} \tag{2}$$

In an early study of zeotropic condensation in finned tubes, Koyama et al. (1990) condensed three binary mixtures of R-22 and R-114, and the individual components in a spirally-grooved tube. The average heat transfer coefficients were lower for the mixtures with a maximum decrease of 20% compared to the pure components. In another study, Shizuya et al. (1995) compared the heat transfer enhancement for four pure refrigerants and three binary mixtures of the pure refrigerants in smooth and finned tubes. They found the heat transfer enhancement associated with the finned tube compensated for the performance reduction associated with the refrigerant mixtures.

Eckels and Tesene (1999a) found that microfin tubes increased heat transfer coefficients by 200% on average at low mass fluxes, and by 50% on average at higher mass fluxes. The greater performance at low mass fluxes was attributed to the fins causing enhanced turbulence in the condensate layer and the delayed transition from annular to wavy flow. In the second part of their investigation, they reported that pressure drop in the microfin tubes increased by 30% to 60% for all refrigerants compared to the smooth tube Eckels and Tesene (1999b). Cavallini et al. (2006) observed optimal condensation heat transfer performance at a mass flux of 200 kg m^{-2} s^{-1} due to the fins producing an extended region

of annular flow. At the highest mass flux tested (800 $kg\,m^{-2}\,s^{-1}$), enhancement factors were all about 1.5. Pressure drop penalty factors were about 2.5 for mass fluxes in the range of 400 to 800 $kg\,m^{-2}\,s^{-1}$.

Several flow visualization studies have been carried for condensation in microfin tubes. Oh and Bergles (2002) used an industrial borescope to observe the condensate flow in a smooth tube and four microfin tubes. For stratified flow, liquid flowed almost continuously to the top of the tube with an 18° spiral angle while liquid did not flow continuously to the top of the tubes with 6° and 44° spiral angles. The time-averaged wall temperature at the top of the 18° tube was lower compared to the other tubes and resulted in higher heat transfer coefficients. Increasing the helix angle from 6° to 44° increased the pressure drop by a maximum of 10%. In another flow visualization study, Mohseni and Akhavan-Behabadi (2011) concluded that the fins inside the tube caused an increase in flow turbulence and created swirling flow patterns. The fins also caused mist formation during annular flow which thinned the liquid film on the circumference of the tube leading to enhanced heat transfer.

3. EXPERIMENTAL APPROACH

3.1 Experimental Facility

The experimental condensation facility, shown in Figure 1, was designed to measure heat transfer coefficients and pressure drop for complete condensation of a refrigerant. The facility and validation procedures have been discussed in detail in Jacob et al. (2019) and Jacob (2020). A summary of facility operation is provided here for completeness. The refrigerant loop consists of a positive-displacement gear pump, an evaporator, the test section, and a post-cooler. The refrigerant pump is magnetically coupled to the drive motor, so no lubricating oil is present in the loop. The refrigerant mass flow rate is measured using a Coriolis-effect mass flow meter. Cartridge heaters vaporize and superheat the refrigerant in the evaporator section. The system pressure in the refrigerant loop is set using a piston accumulator and a nitrogen cylinder. Sight glasses at the inlet and outlet of the test section provide visual verification that the refrigerant is superheated at the inlet and subcooled at the outlet. After exiting the test section, the refrigerant is subcooled in the post-cooler.

The water loop consists of a magnetically coupled, positive displacement gear pump. The water flow rate is measured using a positive displacement volumetric flow meter. The mass flow rate of water through the test section is calculated using the volumetric flow rate and the density of water at the pump outlet, calculated from the measured temperature and pressure. A brazed-plate heat exchanger with an ethylene-glycol solution as the coolant is used to cool the water before it enters the test section.

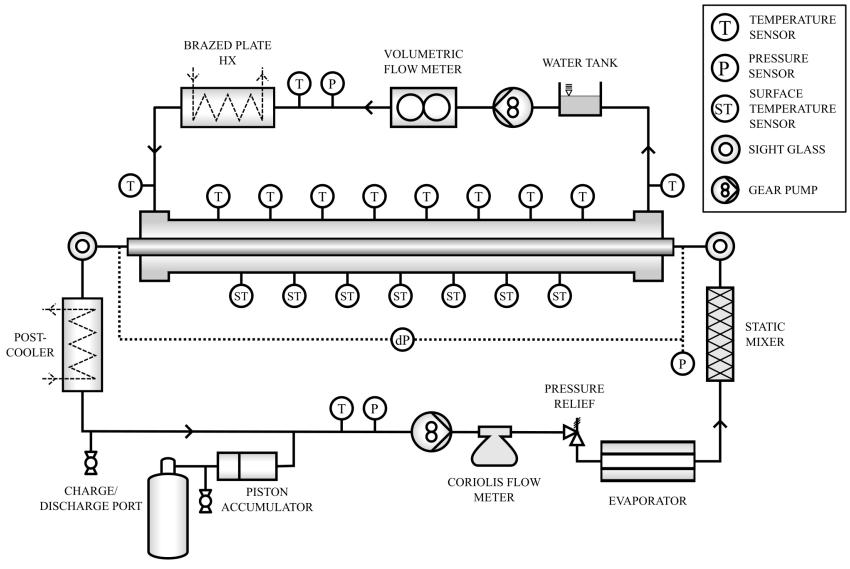

Figure 1: A schematic of the experimental facility.

Table 2: Instrument ranges and uncertainties

Measurement	Range	Systematic Uncertainty
RTD	−200 - 500 °C	±0.05 °C
Surface temperature	−40 - 260 °C	±0.5 °C
T-type thermocouple	−40 - 260 °C	±0.5 °C
Pressure	0 - 10 MPa	±5.68 kPa
Differential pressure	0 - 249 MPa	±0.05 kPa
Refrigerant mass flow meter	0 - 30 g s^{-1}	±0.1 %
Water volumetric flow meter	0.04 - 7.5 L min^{-1}	±0.5 %

3.2 Test Section

The test section is a counter flow, tube-in-tube heat exchanger with water flowing in the annulus and refrigerant flowing in the inner 4 mm OD microfin tube. The wall thickness is 0.18 mm and the surface area ratio is 1.56. The surface area ratio is defined as the actual inner surface area of the microfin tube over the inner surface area of a smooth tube with the same inner diameter, D_i, and is calculated using Equation (3) from Webb and Kim (2005). The characteristic geometries of a microfin tube are shown in Figure 2. Eight RTDs are inserted midway into the annulus to measure the water temperature across the test section. Flow mixers are positioned before and after each water temperature measurement to ensure that the bulk water temperature is measured. The RTDs divide the test section into seven segments, and each segment is 19 cm in length. A rendering of the test section is shown in Figure 2. Two additional RTDs measure the water temperature at the inlet and outlet of the test section. Fine-gauge, bare-bead, T-type thermocouples were soldered to the top surface of the microfin tube at the middle of each segment to measure the surface temperature.

$$\frac{A}{A_p} = 1 + 2\frac{h}{p}\left[\sec\left(\frac{\gamma}{2}\right) - \tan\left(\frac{\gamma}{2}\right)\right] \tag{3}$$

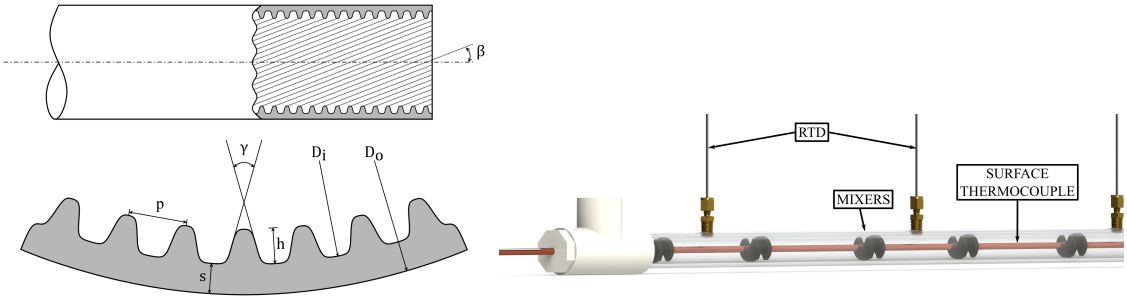

Figure 2: A schematic of microfin geometries (left) and a rendering of the test section (right).

3.3 Instrumentation and Uncertainty Propagation

Three-wire platinum RTDs are used to measure the water temperature across the test section. The surface temperatures of the microfin tube are measured using T-type thermocouples that have an uncertainty of ±0.5 °C as specified by the manufacturer. The refrigerant inlet and outlet temperatures were also measured using T-type thermocouples and had the same uncertainty. The systematic uncertainties for all measurements are shown in Table 1.

Uncertainties in the calculated frictional pressure drop and heat transfer coefficients were calculated using an uncertainty propagation analysis suggested by Kline and McClintock (1953). The uncertainty in the calculated variables is due to systematic and random uncertainties from the temperature, pressure, flow meters and the data acquisition system. Systematic uncertainties, shown in Table 2, were evaluated based on the uncertainty of the sensor, data acquisition system and the calibration process.

4. DATA REDUCTION

Data were collected for each test condition once a steady state was reached. This was achieved when temperature, absolute pressure, and mass flow rate measurements changed by no more than 0.1 °C, 10 kPa and 0.1 g s^{-1}, respectively, for at least four minutes. Data were collected for four minutes at a sampling frequency of 1 Hz, and the time-averaged values were used for calculations.

4.1 Heat Transfer Coefficients

Heat transfer coefficients were calculated for the seven segments in the test section. The refrigerant temperature and pressure are measured at the inlet and outlet of the test section where the refrigerant is superheated and subcooled, respectively. The refrigerant enthalpy at the inlet and outlet are known. Water-side energy balances in each segment are then used to determine the refrigerant enthalpy for each segment in the test section. The heat duty in each segment, Q_i, is calculated using Equation (4), where $\dot{m}_w$ is the water mass flow rate, $c_{p,w}$ is the specific heat of water, and $\Delta T_{w,i}$ is the change in water temperature for a segment. The refrigerant enthalpy, h_r, at the outlet of each segment is calculated using Equation (5), where $\dot{m}_r$ is the refrigerant mass flow rate. The subscript i indicates the segment number. The heat flux, $\dot{q}''$, for a segment is calculated using Equation (6), where D_i is the tube diameter to the fin root.

$$\dot{q}_i = \dot{m}_w \, c_{p,w} \, \Delta T_{w,i} \tag{4}$$

$$h_{r,out,i} = h_{r,in,i} - \frac{\dot{q}_i}{\dot{m}_r} \tag{5}$$

$$\dot{q}'' = \frac{\dot{q}}{\pi D_i L} \tag{6}$$

The inner wall temperature, $T_{wall,in}$, of the microfin tube is calculated using Equation (7), which is the one-dimensional heat conduction equation utilizing the measured outer wall temperature, $T_{wall,out}$. L_i is the length of a segment and k_c is the conductivity of copper.

$$T_{wall,in,i} = T_{wall,out,i} + \frac{\dot{q}_i \ln \frac{D_o}{D_i}}{2\pi L_i k_c} \tag{7}$$

The heat transfer coefficient is calculated as shown in Equation (8) where $T_{r,sat}$ is the equilibrium saturation temperature of the refrigerant at the system pressure.

$$\alpha_i = \frac{\dot{q}''}{T_{r,sat} - T_{wall,in,i}} \tag{8}$$

4.2 Two-phase Frictional Pressure Drop

The differential pressure transducer ports were installed at the inlet and outlet of the microfin tube, as shown in Figure 1. The measured pressure gradient for complete condensation, ΔP_m, includes the pressure change due to deceleration, ΔP_d, of the condensed refrigerant, the frictional pressure drop, ΔP_{fr}, across the tube, and pressure drop due to single-phase flow regions at the inlet, $\Delta P_{fr,v}$, and outlet,$\Delta P_{fr,l}$, of the test section. The frictional pressure gradient is calculated as shown in Equation (9).

$$\Delta P_{fr} = \Delta P_m + \Delta P_d - \Delta P_{fr,v} - \Delta P_{fr,l} \tag{9}$$

The flow deceleration contribution to the overall pressure gradient is evaluated using Equation (10), where $\rho_{r,v}$ and $\rho_{r,l}$ are the vapor and liquid phase densities, respectively.

$$\Delta P_d = \rho_v V_v^2 - \rho_l V_l^2 \tag{10}$$

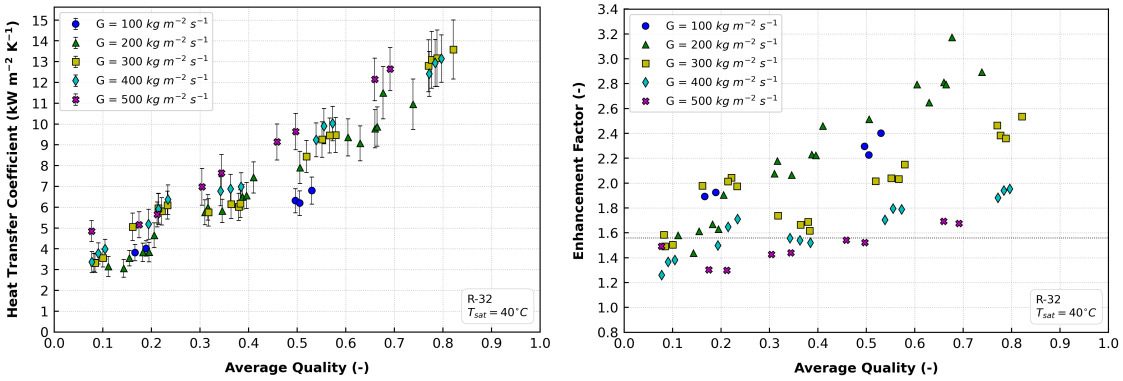

Figure 3: Heat transfer coefficients and enhancement factors for R-32 condensing at 40 °C.

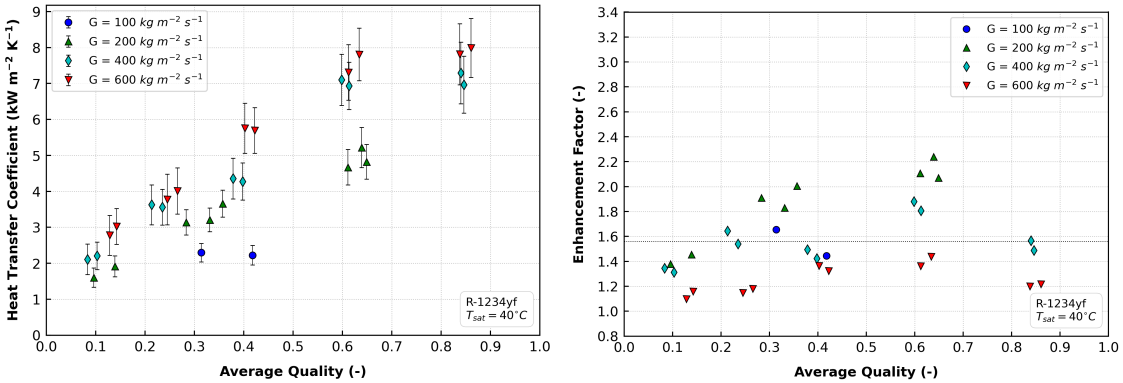

Figure 4: Heat transfer coefficients and enhancement factors for R-1234yf condensing at 40 °C.

The length of the two-phase flow region was determined by fitting a second-order polynomial to the vapor quality and the corresponding axial position along the microfin tube, as described in Jacob et al. (2019). The physical location where condensation started and ended was determined by evaluating the polynomial at vapor qualities of 1 and 0, respectively. The lengths over which single-phase vapor and liquid flows occurred were estimated using the known length of the microfin tube. The single-phase frictional pressure drops were evaluated using the correlation by Ravigururajan and Bergles (1996) using the hydraulic diameter of the microfin tube rather than the maximum inside diameter as suggested by Wu and Sundén (2016). Single-phase experiments were conducted prior to this investigation to verify the accuracy of the modification proposed by Wu and Sundén (2016). The correlation predicted experimental single-phase frictional pressure drops with a mean average percent error (MAPE) of 7% for Reynolds numbers from 2,500 to 30,000.

5. RESULTS

Condensation heat transfer coefficients and frictional pressure drops were measured for R-454C and R-1234yf at saturation temperatures of 40, 50, and 60 °C and mass fluxes from 100 to 600 kg m^{-2} s^{-1}. Heat transfer and pressure drop data were obtained for R-32 at a saturation temperature of 40 °C for mass fluxes from 100 to 500 kg m^{-2} s^{-1} due to pressure limitations of the test facility.

5.1 Heat Transfer Coefficients

Generally, the heat transfer coefficients increase with mass flux and vapor quality as shown in Figures 3, 4 and 5. As saturation temperatures increase from 40 to 60 °C, the heat transfer coefficients decrease, as expected. R-32 has the highest heat transfer coefficients of the three refrigerants due to its high liquid thermal conductivity. To calculate the enhancement factor, the smooth tube diameter in this investigation is set equal to the root diameter of the microfin tube, as shown in Figure 2. The smooth tube heat transfer coefficients are calculated using a correlation developed by

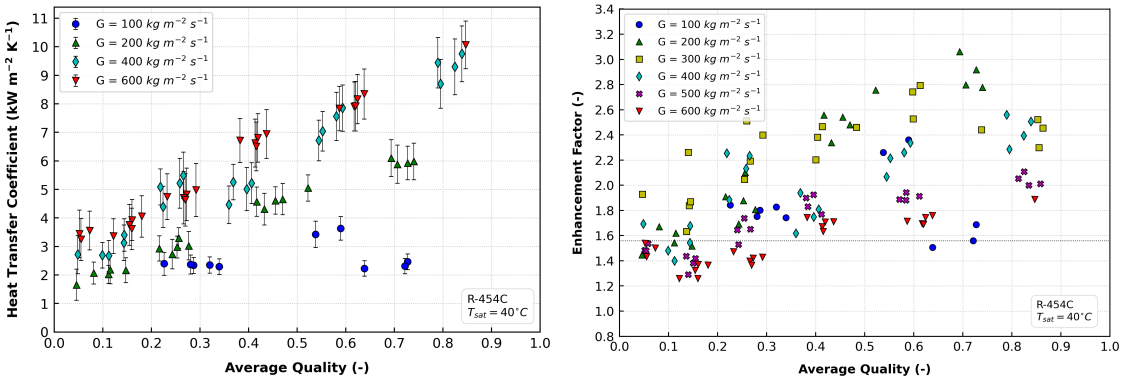

Figure 5: Heat transfer coefficients and enhancement factors for R-454C condensing at 40 °C.

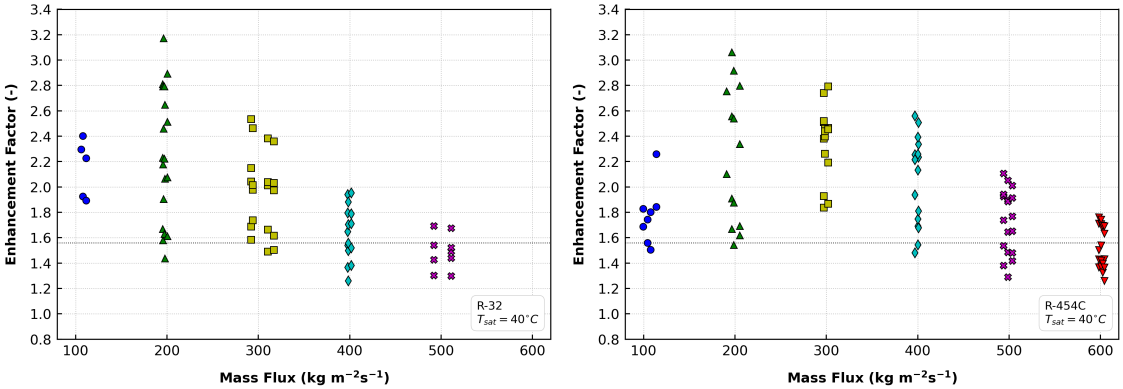

Figure 6: Enhancement factors plotted against mass flux for R-32 and R-454C condensing at 40 °C

Cavallini et al. (2006). The increase in surface area for the microfin tube, represented as an area ratio, is estimated using an equation presented by Webb and Kim (2005), and is 56% greater than the similar smooth tube. The area ratio is plotted for reference with a dashed line in the figures that show the enhancement factor. The enhancement factor tends to increase with vapor quality as shown in the plots on the right of Figures 3, 4 and 5. This trend is observed because as the vapor quality decreases, the inter-fin region fills with condensate, and eventually the condensate layer rises above the fins and the inter-fin region remains flooded. Before the onset of flooding, the fins drain condensate from the fin tip to the trough region leaving a thin layer of condensate at the tip of the fin. The thinner layer of condensate results in a reduced thermal resistance between the cooled surface and the bulk flow which produces high heat transfer coefficients.

The effect of mass flux on the enhancement factor is made clear in the plots shown in Figure 6. The enhancement factors for all fluids tend to increase with mass flux up to around 200 $\mathrm{kg\,m^{-2}\,s^{-1}}$ and then decrease as mass flux increases to 600 $\mathrm{kg\,m^{-2}\,s^{-1}}$. This trend is shown for R-32 and R-454C in Figure 6. Pronounced enhancement at low mass fluxes is due to the redistribution of condensate around the circumference of the tube, surface tension driven drainage from the fin tips to the trough region, and the increased interfacial turbulence caused by the fins (Wu et al., 2014). Kedzierski and Goncalves (1999) attributed the enhancement at low mass fluxes to the reduction in size of the turbulent eddies at the wall which is caused by the fins. Smaller eddies transport momentum more effectively, and large eddies are not as common in high Reynolds number flows. The maximum enhancement factor in this study is 3.2 which occurred at a mass flux of about 200 $\mathrm{kg\,m^{-2}\,s^{-1}}$ with R-32, as shown in Figure 6.

5.2 Frictional Pressure Drop

The correlation developed by Müller-Steinhagen and Heck (1986) is used to calculate the smooth tube condensation frictional pressure drop. The penalty factors for R-32 and R-454C are shown in Figure 8 for the range of mass fluxes tested. The penalty factors for R-454C range from 1.0 to 3.0 for the range of mass fluxes tested, as shown in Figure 8.

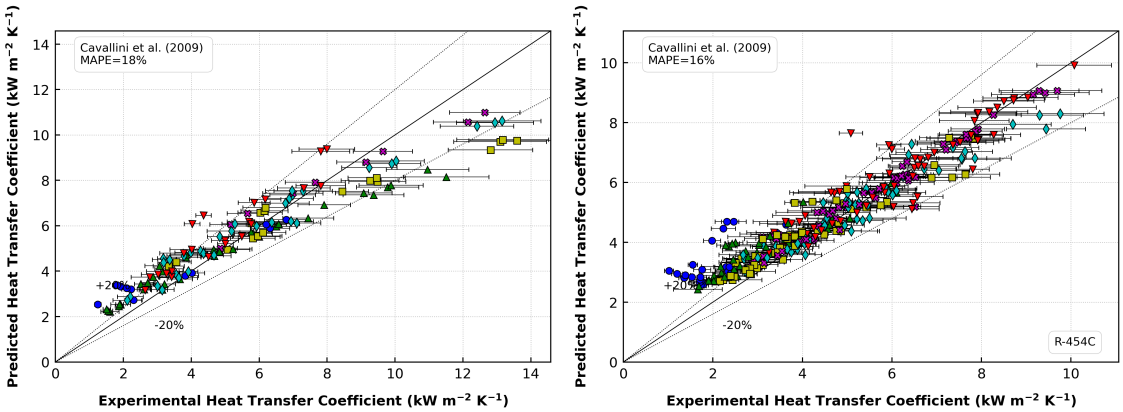

Figure 7: Predicted versus experimental heat transfer coefficients for the pure fluids R-32 and R-1234yf (left) and the mixture R-454C (right) condensing at 40 °C.

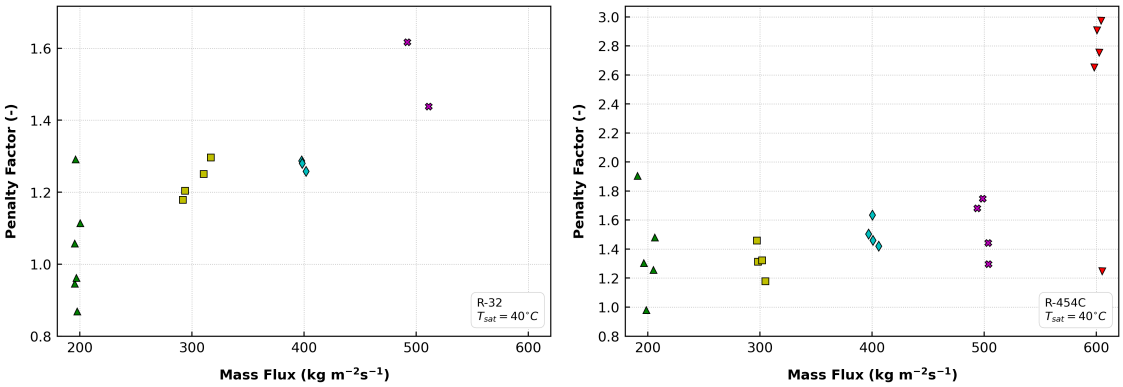

Figure 8: Penalty factors for R-32 (left) and R-454C (right) condensing at 40 °C.

The average PF for mass fluxes from 200 to 500 kg m^{-2} s^{-1} is 1.4, 1.2, and 1.3 for R-454C and R-32, and R-1234yf, respectively. Penalty factors tend to increase with mass flux, as expected. The observed trends for enhancement factor and penalty factor suggest the optimum operating conditions for this tube occurs at low mass fluxes where maximum enhancement factors occur with minimal increase in penalty factor.

5.3 Evaluation of Correlations

The predictive performance of three heat transfer and three frictional pressure drop correlations were evaluated for the test conditions in this investigation. Figure 7 shows a comparison of all experimentally calculated heat transfer coefficients and the heat transfer coefficients calculated by the Cavallini et al. (2009) microfin correlation for the pure fluids (left) and the mixture (right). The plot markers indicate the mass flux the data point was taken at, and are kept consistent with other plots. The heat transfer correlation developed by Cavallini et al. (2009) is the most accurate with a mean average percent error (MAPE) of 18% and 16% for the pure fluids and the mixture, respectively, as shown in Figure 7. The dashed lines represent deviations of ± 20% from the experimentally calculated heat transfer coefficients. The Silver-Bell-Ghaly (SBG) correction was applied to calculate heat transfer coefficients for the mixture, however, the Cavallini et al. (2009) correlation performed slightly better without the correction applied. The frictional pressure drop correlation developed by Han and Lee (2005) performed the best and predicted the experimental data with a MAPE of 33%, as shown in Figure 9. The frictional pressure drop data for both the pure fluids and the mixture are shown. The development of the Han and Lee (2005) and Cavallini et al. (2009) correlations included data for smaller diameter tubes (from 4 to 7 mm) which is likely why they performed better than other correlations available in the literature.

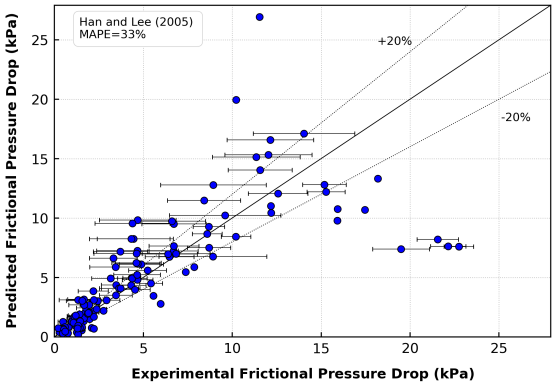

Figure 9: Comparison of predicted versus experimental frictional pressure drop for all fluids.

6. CONCLUSION

This paper compares the condensation heat transfer and pressure drop for zeotropic refrigerant R-454C and its individual components, R-32 and R-1234yf, in a horizontal microfin tube. The microfin tube has a 4 mm OD, 0.18 mm wall thickness, and a surface area ratio of 1.56. Condensation heat transfer coefficients and frictional pressure drops were calculated for R-454C and R-1234yf at saturation temperatures of 40, 50, and 60 °C and mass fluxes from 100 to 600 $\mathrm{kg\,m^{-2}\,s^{-1}}$. Heat transfer and pressure drop data were taken for R-32 at a saturation temperature of 40 °C for mass fluxes from 100 to 500 $\mathrm{kg\,m^{-2}\,s^{-1}}$. R-32 had the highest enhancement factor of 3.2 at a mass flux of 200 $\mathrm{kg\,m^{-2}\,s^{-1}}$, while penalty factors at this mass flux ranged from 0.9 to 1.3. For R-1234yf, enhancement factors ranged from 0.9 to 2.2, and penalty factors ranged from 1.1 to 4.0. Enhancement factors for R-454C ranged from 1.2 to 3.1 and penalty factors ranged from 1.1 to 3.1. Penalty factors increased with mass flux while enhancement factors initially increase from 100 to 200 $\mathrm{kg\,m^{-2}\,s^{-1}}$, and then decrease with further increase in mass flux. These trends suggest that microfin tubes perform the best at low mass fluxes. Based on the data collected in this investigation, the authors suggest using the heat transfer correlation developed by Cavallini et al. (2009) and the frictional pressure drop correlation developed by Han and Lee (2005).

REFERENCES

Bashar, M. K., Nakamura, K., Kariya, K., and Miyara, A. (2020). Condensation heat transfer of R1234yf in a small diameter smooth and microfin tube and development of correlation. *International Journal of Refrigeration*, 120:331–339.

Cavallini, A., Censi, G., Col, D. D., Doretti, L., Rossetto, L., and Longo, G. A. (2002). Heat Transfer Coefficients Of HFC Refrigerants During Condensation At High Temperature Inside An Enhanced Tube. page 10, Purdue University.

Cavallini, A., Col, D. D., Mancin, S., and Rossetto, L. (2006). Thermal Performance of R410A Condensing in a Microfin Tube. page 10, Purdue University.

Cavallini, A., Del Col, D., Mancin, S., and Rossetto, L. (2009). Condensation of pure and near-azeotropic refrigerants in microfin tubes: A new computational procedure. *International Journal of Refrigeration*, 32(1):162–174.

Diani, A., Campanale, M., Cavallini, A., and Rossetto, L. (2018). Low GWP refrigerants condensation inside a 2.4 mm ID microfin tube. *International Journal of Refrigeration*, 86:312–321.

Eckels, S. J. and Tesene, B. A. (1999a). A Comparison of R-22, R-134a, R-410a, and R-407c Condensation Performance in Smooth and Enhanced Tubes: Part I, Heat Transfer. *ASHRAE Transactions: Research*, 105(2):428–441.

Eckels, S. J. and Tesene, B. A. (1999b). A comparison of R-22, R-134a, R-410a, and R-407c condensation performance in smooth and enhanced tubes: Part II, pressure drop. In *ASHRAE Transactions*, volume 105, pages 442–452.

Han, D. and Lee, K.-J. (2005). Experimental study on condensation heat transfer enhancement and pressure drop penalty factors in four microfin tubes. *International Journal of Heat and Mass Transfer*, 48(18):3804–3816.

Hirose, M., Ichinose, J., and Inoue, N. (2018). Development of the general correlation for condensation heat transfer and pressure drop inside horizontal 4 mm small-diameter smooth and microfin tubes. *International Journal of*

Refrigeration, 90:238–248.

Jacob, T. A. (2020). *Investigation of In-tube Non-equilibrium Condensation of Low Global Warming Potential Refrigerants*. PhD thesis, Oregon State University.

Jacob, T. A., Matty, E. P., and Fronk, B. M. (2019). Experimental investigation of in-tube condensation of low GWP refrigerant R450A using a fiber optic distributed temperature sensor. *International Journal of Refrigeration*, 103:274–286.

Kedzierski, M. A. and Goncalves, J. M. (1999). Horizontal Convective Condensation of Alternative Refrigerants Within a Micro-Fin Tube. *Enhanced Heat Transfer*, 6:161–178.

Kim, M.-H. and Shin, J.-S. (2005). Condensation heat transfer of R22 and R410A in horizontal smooth and microfin tubes. *International Journal of Refrigeration*, 28(6):949–957.

Kline, S. J. and McClintock, F. A. (1953). Describing uncertainties in single-sample experiments. *Mechanical Engineering*, pages 3–8.

Kondou, C. (2019). Heat transfer and pressure drop of R1123/R32 (40/60 mass%) flow in horizontal microfin tubes during condensation and evaporation. *Science and Technology for the Built Environment*, 25(10):1281–1291.

Koyama, S., Miyarat, A., Takamatsu, H., and Fujii, T. (1990). Condensation heat transfer of binary refrigerant mixtures of R22 and Rl14 inside a horizontal tube with internal spiral grooves. *International Journal of Refrigeration*, 13:8.

Mohseni, S. and Akhavan-Behabadi, M. (2011). Visual study of flow patterns during condensation inside a microfin tube with different tube inclinations. *International Communications in Heat and Mass Transfer*, 38(8):1156–1161.

Müller-Steinhagen, H. and Heck, K. (1986). A simple friction pressure drop correlation for two-phase flow in pipes. *Chemical Engineering and Processing: Process Intensification*, 20(6):297–308.

Oh, S.-Y. and Bergles, A. E. (2002). Visualization of the Effects of Spiral Angle on the Enhancement of In-Tube Flow Boiling in MicrofinTubes. In *ASHRAE Transactions*, volume 108, pages 509–515.

Ravigururajan, T. and Bergles, A. (1996). Development and verification of general correlations for pressure drop and heat transfer in single-phase turbulent flow in enhanced tubes. *Experimental Thermal and Fluid Science*, 13(1):55–70.

Shizuya, M., Itoh, M., and Hijikata, K. (1995). Condensation of Nonazeotropic Binary Refrigerant Mixtures Including R22 as a More Volatile Component Inside a Horizontal Tube. *Journal of Heat Transfer*, 117(2):538–543.

Webb, R. L. and Kim, N.-H. (2005). *Principles of Enhanced Heat Transfer*. Taylor & Francis, 2 edition.

Wu, Z. and Sundén, B. (2016). Frictional Pressure Drop Correlations for Single-Phase Flow, Condensation, and Evaporation in Microfin Tubes. *Journal of Heat Transfer*, 138(2):022901.

Wu, Z., Sundén, B., Wang, L., and Li, W. (2014). Convective Condensation Inside Horizontal Smooth and Microfin Tubes. *Journal of Heat Transfer*, 136(5):051504.

ACKNOWLEDGMENT

The authors would like to thank Wieland-Werke AG for providing the microfin tube used in this investigation.